IMPACT OF TYPHOONS ON THE OCEAN IN THE PACIFIC

BY E.A. D'ASARO, P. G. BLACK, L. R. CENTURIONI, Y.-T. CHANG, S. S. CHEN, R. C. FOSTER, H. C. GRABER, P. HARR, V. HORMANN, R.-C. LIEN, I.-I. LIN, T. B. SANFORD, T.-Y. TANG, AND C.-C. WU

The interactions between typhoons and the ocean vary greatly depending on the properties of the storm and of the ocean.

T ropical cyclones (TCs) interact with both the atmosphere and the upper ocean. They draw their energy from the warm ocean, but in doing so also change the ocean in a broad swath around their track by direct cooling and through the action of the ocean waves and currents generated by TC winds (Leipper 1967; Price 1981; Black 1983; Shay 2010; and references therein). This affects the evolution of the TC and also leaves an imprint on the ocean that can last long after the storm has passed. The Impact of Typhoons on the Ocean in the Pacific/Tropical Cyclone Structure 2010 (ITOP/TCS10) program combined intensive meteorological and oceanographic observations of TCs in the western North Pacific to study these interactions and compare them to previous measurements in the Atlantic (e.g., Black et al. 2007) and Gulf of Mexico (e.g., Jaimes and Shay 2009, 2010)

ITOP GOALS. *How does the cold wake of a typhoon form and dissipate?* Typhoons produce a complex three-dimensional response in the underlying ocean including strong mixed layer currents, upwelling of the thermocline, intense mixing across the thermocline, generation and propagation of near-inertial internal waves, and the formation of a cold wake beneath the storm. The cold wake persists after the typhoon passage (Pudov and Petrichenko 2000), modifying the air–sea interaction and the biogeochemistry of the upper ocean (Shay 2010; Lévy et al. 2012; and references therein), and decaying through a poorly known combination of air–sea flux and

AFFILIATIONS: D'ASARO, LIEN, AND SANFORD—Applied Physics Laboratory, and School of Oceanography, University of Washington, Seattle, Washington; BLACK—Science Application International Corporation, Inc., and Naval Research Laboratory, Monterey, California; CENTURIONI AND HORMANN—Scripps Institution of Oceanography, University of California, San Diego, La Jolla, California; CHANG AND TANG—Institute of Oceanography, National Taiwan University, Taipei, Taiwan; CHEN AND GRABER—Rosenstiel School of Marine and Atmospheric Science, University of Miami, Miami, Florida; FOSTER—Applied Physics Laboratory, University of Washington, Seattle, Washington; HARR—Naval Postgraduate School, Monterey, California; LIN—Department of Atmospheric Sciences, National Taiwan University, and Research Center for Environmental Changes, Academia Sinica, Taipei, Taiwan; WU—Department of Atmospheric Sciences, National Taiwan University, Taipei, Taiwan

CORRESPONDING AUTHOR: E. A. D'Asaro, University of Washington, Applied Physics Laboratory, 1013 NE 40th St., Seattle, WA 98105
E-mail: dasaro@apl.washington.edu

mixing processes. Although previous observations have shown cold wakes reappearing in SST observations after a period of warming (e.g., Price et al. 2008), detailed observations of this phenomenon are rare, with subsurface observations mostly focusing on the first few days of evolution.

ITOP aimed to measure the ocean response to typhoons in detail, particularly the formation and dissipation of the cold wake, and to compare these measurements with the predictions generated by numerical models.

What are the air–sea fluxes for winds greater than 30 m s^{-1}? TCs draw their energy from the underlying warm ocean and thus tend to be more intense if the fluxes of heat and moisture from the ocean are greater (Emanuel 1999). They are damped by drag on the ocean and thus tend to be less intense if the drag is greater. Although the drag coefficient is now believed to remain constant or decrease at high wind speeds (Black et al. 2007), large uncertainties among different observations and parameterizations of momentum, heat, and moisture exchange rates remain. ITOP aimed to make additional measurements, at higher wind speeds, and under a larger variety of atmospheric and oceanic conditions.

How does the ocean stratification and its variability affect the ocean response to typhoons? Variability in the ocean thermal structure due to regional differences

and to transient variations caused by ocean eddies is expected to modify the air–sea fluxes and thus TC intensity. Regions with warm, deep upper layers may act as typhoon boosters by limiting the amount of cooling beneath the storm, and those with cold, shallow upper layers correspondingly act as typhoon dampers (e.g., Hong et al. 2000; Lin et al. 2005, 2008). Eddy currents may complicate these interactions (Yablonsky and Ginis 2013). We expect eddy effects to be stronger in the western Pacific than in the Atlantic because the typical sea surface height variability in the western Pacific is 50%–100% larger than in the open western Atlantic. ITOP aimed to study these interactions in detail.

How do surface waves affect air–sea interactions beneath typhoons? Surface wave fields beneath typhoons are complex, with multiple dominant wave directions varying and interacting across the different storm quadrants (Wright et al. 2001). The new generation of coupled TC models includes explicit wave fields from which the air–sea heat and momentum fluxes are computed (Chen et al. 2007, 2013). More practically, the surface waves produced by typhoons are of great interest in themselves, especially relevant in marine and impact forecasting. ITOP aimed to measure the surface wave field underneath typhoons, to compare these measurements with models, and to assess their impact on air–sea exchange and remote sensing signatures.
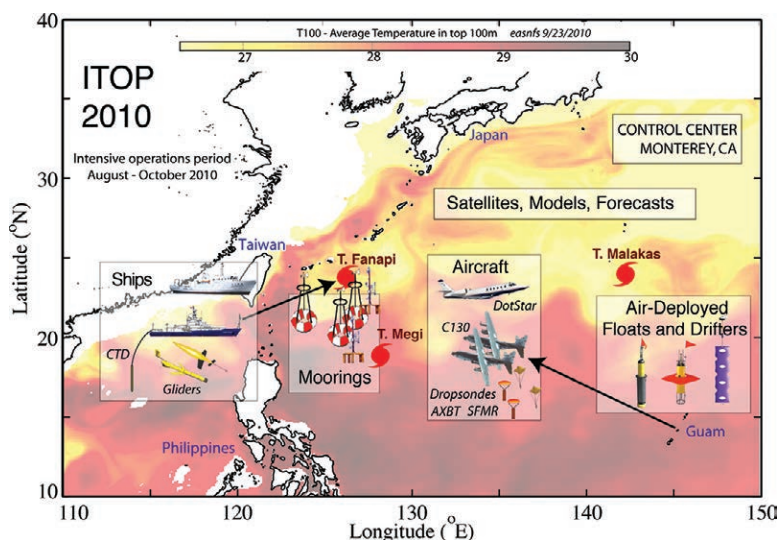

Fig. 1. **Background color map of T100, the average temperature in the upper 100 m of the ocean, from the East Asia Seas Nowcast/Forecast System on 23 Sep 2010. Overlaid are graphical representations of the ITOP operations area, experimental tools, and strategy. Locations of the three major ITOP storms at the time of maximum sampling are shown by storm symbols.**

EXPERIMENTAL SETTING, TOOLS, AND STRATEGY. The experiment focused on the western tropical North Pacific, a region with the highest climatological density of typhoons. This region has strong north–south gradients in ocean stratification (Fig. 1) but not SST (Fig. 2). The average temperature in the upper 100 m of the ocean (T100) is a simple estimate of the expected surface temperature after typhoon mixing (Price 2009). In the south, T100 averages 30°C, only about 0.5°C less than the surface temperature before typhoon mixing; here, mixing by typhoons will cause very little ocean cooling and will have little effect on the air–sea temperature difference during TCs. In the north, T100 reaches 26°C, about 3.5°C less than the surface temperature before

typhoon mixing; here typhoon-induced mixing will cause strong ocean cooling and is more likely to reduce the air–sea temperature difference beneath TCs. Between roughly 19° and 22°N T100, and thus the ocean feedback to TCs, is highly variable due to strong ocean eddies (Lin et al. 2005, 2008).

The ITOP experimental strategy used both traditional and newly developed tools to sample oceanic and atmospheric variability on a variety of space and time scales (Fig. 1). During an intensive observation period (August–October 2010), detailed measurements of typhoons and the immediate ocean response were made using aircraft. Two WC-130J "Hurricane Hunter" aircraft were operated by the Air Force Reserve Command 53rd Weather Reconnaissance Squadron from Guam, and an Astra jet aircraft was operated by the Dropwindsonde Observations for Typhoon Surveillance near the Taiwan Region (DOTSTAR) program (Wu et al. 2005). The WC-130s penetrated the storms during reconnaissance flights, observing their structure and that of the underlying ocean. Dropsondes measured wind, air temperature, and humidity; a microwave sensor, the Stepped Frequency Microwave Radiometer (SFMR; Uhlhorn et al. 2007), measured surface wind and rainfall; and airborne expendable bathythermographs (AXBTs) measured the ocean temperature in the upper 500–800 m. The Astra conducted surveillance flights in the environment around storms approaching Taiwan using dropsondes. More detailed and extended measurements of the ocean and of the atmospheric boundary layer were made using a new generation of autonomous oceanographic instruments developed during the Coupled Boundary Layer Air–Sea Transfer (CBLAST) program (Black et al. 2007). A total of 81 Electromagnetic Autonomous Profiling Explorer (EM-APEX) floats (Sanford et al. 2011), Lagrangian floats (D'Asaro and McNeil 2007), and several varieties of surface drifters (Niiler 2001; Black et al. 2007; Centurioni 2010) were deployed in specially designed air-launch packages from a WC-130 aircraft. Arrays of these instruments were deployed in front of typhoons Fanapi and Megi and measured the evolution of ocean temperature, salinity, and velocity through each storm's passage and for longer than one month afterward. Some instruments also measured surface pressure, surface waves, and ocean boundary layer turbulence. Additional instruments deployed after the passage of typhoons Fanapi and Malakas measured the long-term evolution of the storm wakes.

A longer-term context was provided by moorings deployed off Taiwan from March 2009 to November
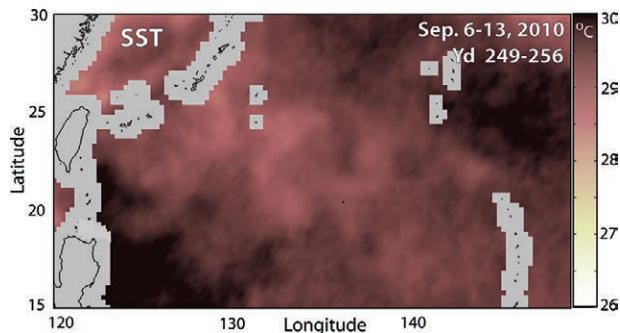

FIG. 2. Mean sea surface temperature, 6–13 Sep 2010, just before the genesis of Typhoon Fanapi. Color scale is as in Fig. 1, demonstrating the lack of SST contrast. Data from the Optimally Interpolated (OI) SST product produced by Remote Sensing Systems.

2010 (Pun et al. 2011). Four surface buoy moorings and three subsurface moorings measured surface meteorology and ocean structure in the upper 500 m. During the intensive observation period, these moorings were supplemented by two highly instrumented, tandem air–sea interaction and surface wave moorings, combining a robust surface platform [the Extreme Air–Sea Interaction (EASI) buoy] with a spar buoy [the Air–Sea Interaction Spar (ASIS)] (Graber et al. 2000). The moored array measured the response to four storms.

The research vessels *Revelle, Ocean Researcher 1,* and *Ocean Researcher 3* were used to deploy and recover the moorings and to study the evolution of the storm wakes on time scales of days to many weeks. During the intensive observation period R/V *Revelle* was initially poised near Taiwan conducting other research and was mobilized rapidly as ITOP's first storm, Typhoon Fanapi, formed. The R/V *Revelle* made detailed surveys of the wakes of Fanapi and Megi and deployed 10 autonomous gliders (Eriksen et al. 2001) to measure ocean temperature and salinity and ocean mixing rates and conducted studies of the biogeochemical properties of the wake. The gliders continued surveying the wake for another 50 days. Gliders, floats, some drifters, and the moorings were recovered by the research vessels after the end of the intensive period.

Synthetic aperture radar (SAR) images from seven satellites (including *Envisat, TerraSAR-X, COSMO-SkyMed*, and *RadarSat-2*) provided coverage of the typhoons in different stages of development. Close cooperation between the ITOP Operations Center and the Center for Southeastern Tropical Advanced Remote Sensing (CSTARS), the satellite downlink facility, resulted in multiple eye images of all three ITOP storms. SAR satellite data were used to generate

TABLE 1. ITOP tropical cyclone properties. Inner core structure parameters of eyewall slope and slant reduction factor are averaged over all passes through the core during an aircraft mission near the time of maximum intensity (with maximum wind tilt angle from vertical in parentheses).

|	12W	13W	15W
Storm ID	12W	13W	15W
Storm name	Typhoon Fanapi	Typhoon Malakas	Supertyphoon Megi
Mission IDs	0420–0620	0222–0422	0330–0830
ITOP observation period (2010)	14–20 Sep	20–25 Sep	13–23 Oct
Maximum SFMR surface wind (kt)	115	90	183
Average flight level R_{max} (nm)	22	45	9
Minimum pressure (mb)	930	948	890
Average ratio: R_{max} sfc to R_{max} 700 mb	0.81 ± 0.09	0.72 ± 0.14	0.94 ± 0.14
V_{max} slope/tilt (°)	0.39 (79)	0.13 (83)	1.85 (46)
Average slant reduction ratio: V_{max} sfc to V_{max} 700 mb	0.88 ± 0.07	0.80 ± 0.20	0.92 ± 0.04
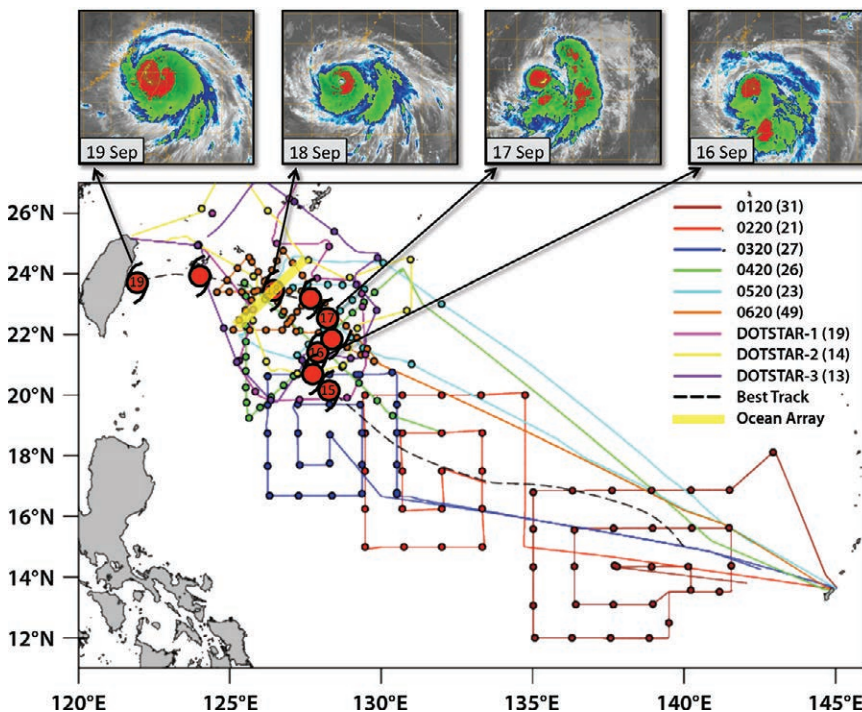
Fig. 3. Aircraft flight tracks and the best track of Typhoon Fanapi. Each WC-130J aircraft mission is defined as xx20, where xx is the mission number and 20 represents the ITOP reference number for the pre-Fanapi disturbance. The DOTSTAR missions are labeled sequentially. The number in parentheses following each aircraft mission label defines the number of dropwindsondes deployed during the mission. The dropwindsonde deployment locations are defined by the circles along each flight track. The dashed line defines the track of the pre-Fanapi disturbance (www.usno.navy.mil/JTWC/). Tropical cyclone symbols begin at the time that the tropical cyclone reached tropical storm intensity and are placed at 12-h intervals. A Multi-functional Transport Satellite (MTSAT; Japan Meteorological Agency) infrared image is provided at each 0000 UTC time. A yellow line shows the deployment line of oceanographic floats and drifters.

described by Patoux et al. (2008) as modified by Foster (2013), and wave fields (Schulz-Stellenfleth and Lehner 2004). SAR observed ubiquitous lines of enhanced wind stress curl aligned along the wind (Foster 2013) and made detailed descriptions of the storms' inner core.

An ITOP operations center at the Naval Postgraduate School in Monterey, California, coordinated the operations and issued customized forecasts for the program. A real-time data system presented analyses and model predictions of the atmosphere and ocean and displayed the locations and data from ITOP measurement systems. Atmospheric data and atmospheric model forecast products were archived and displayed by the National Center for Atmospheric Research Earth Observing Laboratory (NCAR/EOL; http://catalog.eol.ucar.edu /itop_2010/). Oceanic data, both in situ and remotely sensed, and ocean model forecast products were displayed primarily through a data system (https://

high-resolution wind fields (Horstmann et al. 2000, 2005, 2013; Romeiser et al. 2013; Wackerman et al. 1996), surface pressure fields using the method

) at the Monterey Bay Aquarium Research Institute (MBARI). These systems used multiple sources for each of the critical decision quantities (storm track, storm intensity, ocean stratification, and expected ocean response) and displayed these in a uniform manner. The entire system was tested in the fall of 2009—one year before the actual program.

OVERVIEW OF THE ITOP STORMS.

Tropical cyclone activity in the western Pacific was severely suppressed in 2010, with a weak monsoon trough over the Philippine Sea typical of La Niña conditions. Only 14 named storms occurred, compared to an average of 32. Three typhoons were observed extensively during the ITOP program (Table 1); each was spaced fortuitously so as to allow the evolution of storm wakes to be studied without the interference of subsequent storms.

Typhoon Fanapi (Fig. 3) grew from a tropical depression first defined on 1200 UTC 14 September. Three aircraft missions surveyed the storm environment to study its intensification and to provide additional data for the forecast models. Fanapi intensified in an environment of low vertical wind shear to a tropical storm on 0000 UTC 15 September and a typhoon on 1200 UTC 16 September. During this time, the track was complex, turning from northwest to northeast during the tropical storm to typhoon intensification and then back to west as a trough passed. On 17 September, while the storm was still tracking northeastward, a 350-km-long line of floats and drifters was deployed across the forecast storm track in anticipation of the westward turn. This flight, and two more, surveyed the storm as it passed through the middle of the array and reached maximum strength (105 kt; 1 kt = 0.51 m s^{-1}) on 18 September.

Additional flights deployed drifters into the storm wake. Meanwhile, on 16 September, the R/V *Revelle* was recalled to Taiwan; scientists arrived at the ship on 18–19 September just before Fanapi passed over Taiwan. The ship left Kaohsiung harbor on 20 September and reached the cold wake of the storm on 22 September, 4 days after the storm. The ship surveyed the wake until 9 October; gliders deployed from
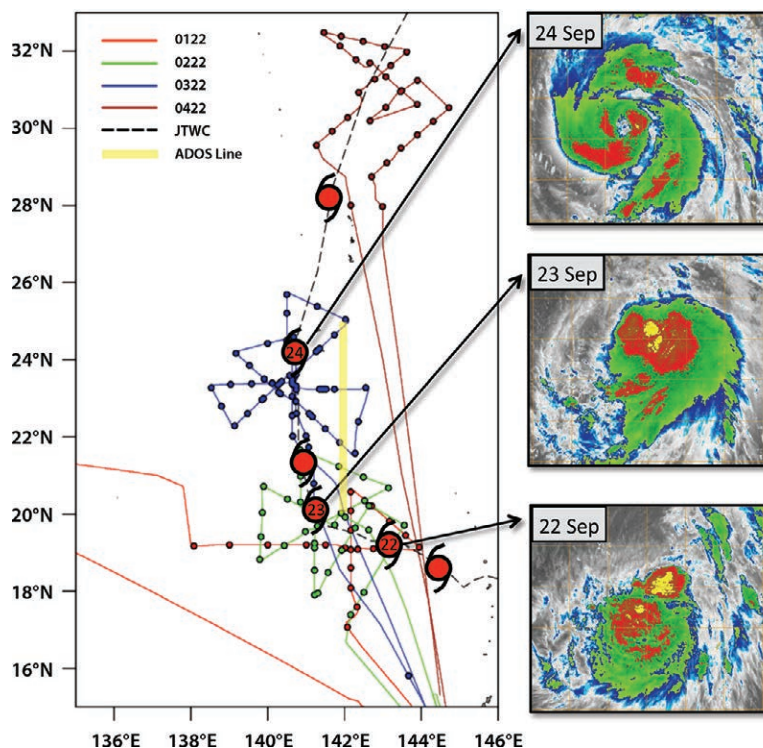

Fig. 4. As in Fig. 3, but for Typhoon Malakas.

the ship continued to survey until about 21 October; drifters continued for much longer.

Typhoon Malakas (Fig. 4) developed as a tropical depression on 20 September as Typhoon Fanapi passed across the Taiwan Straits. The final Fanapi wake flight was diverted to make an initial survey of Malakas. The storm tracked northward during 22 and 23 September, but strong vertical wind shear from the north slowed intensification. As the wind shear relaxed on 24 September, maximum winds of 90 kt occurred and an extratropical transition began. These changes were documented in three flights on 23–25 September. Aircraft operations and oceanographic deployments were limited by the storm's passage close to Iwo-To and other Japanese islands. However, *RadarSat-2* imaged Typhoon Malakas on 22 and 24 September, yielding detailed maps of the wind and pressure fields (Fig. 5). On 29 September, after the storm had passed, six drifters were deployed into the wake along with an extensive AXBT wake survey.

Typhoon Megi (Fig. 6) grew from an area of organized convection, becoming a tropical depression as it passed south of Guam on 1800 UTC 12 October. Six WC-130J and one DOTSTAR flight measured its growth to tropical storm on 0600 UTC 13 October, to typhoon on 1200 UTC 14 September, and to one of the strongest supertyphoons ever recorded on 0240 UTC 17 October. Forecasts of Megi's turn from
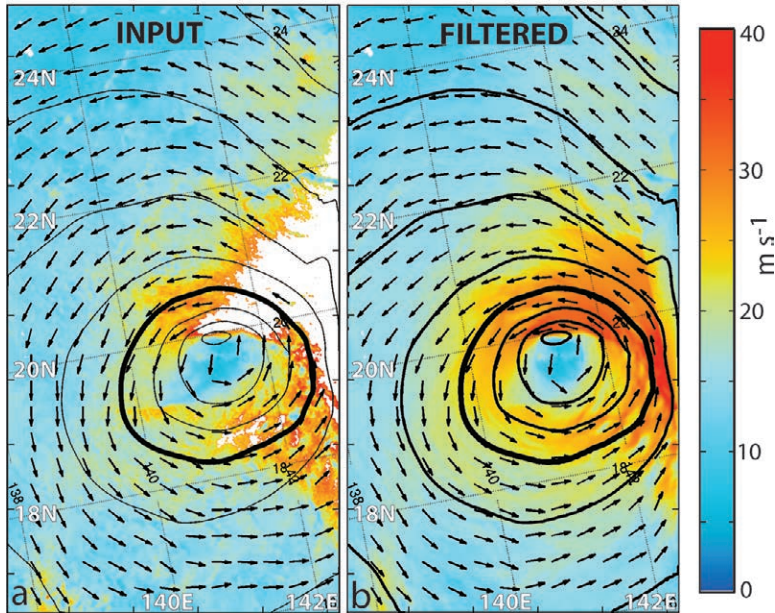
FIG. 5. Winds and pressure fields derived from *RadarSat-2* synthetic aperture radar (SAR) images for Typhoon Malakas on 22 Sep 2010. (a) SAR winds speed (colors) and direction (arrows) computed from SAR image (Horstmann et al. 2000, 2005; Wackerman et al. 1996; Foster 2013). Pressure fields (contours) are computed from winds and referenced to aircraft measurements (Patoux et al. 2008). (b) As in (a), but using a planetary boundary layer model to produce a scene-optimized wind field. Winds and pressures are calculated for 1-km pixels; wind directions are shown every 40 km.

FIG. 6. As in Fig. 3, but for Typhoon Megi.

northwestward to southwestward on 16–17 October contained large uncertainty. Nevertheless, a 200-km-long line of oceanographic floats was deployed perpendicular to the track on 16 October; the storm passed over the southern edge of that array later that day. The final ITOP flight measured Megi's cold wake in the region of peak intensity using air-deployed expendable current, temperature, and salinity (AXCP, AXBT, and AXCTD) probes. Megi then crossed the Philippines and re-emerged in the South China Sea, out of range for the survey aircraft, creating an unusually cold ocean wake (described in the section "Ocean Responses to the ITOP Storms"). A total of 10 synthetic aperture radar images of Typhoon Megi's core were collected from four different satellites (Fig. 7).

COMPARISON OF THE ITOP STORMS.

The three storms occurred in diverse oceanic and atmospheric conditions. Supertyphoon Megi intensified over deep, warm mixed layers with high T100 values; Typhoon Malakas moved northward into a region of colder, shallower mixed layers and lower T100 values; and Typhoon Fanapi transited through the intermediate eddy-rich region. Fanapi and Megi formed from long-lived low-level circulations that moved westward in a nearly uniform easterly flow with intensification occurring steadily over a period of days under the influence of favorable ocean conditions and low to moderate vertical wind shear. Following formation, the two storms moved westward in similar atmospheric environments, but differing oceanic conditions. The
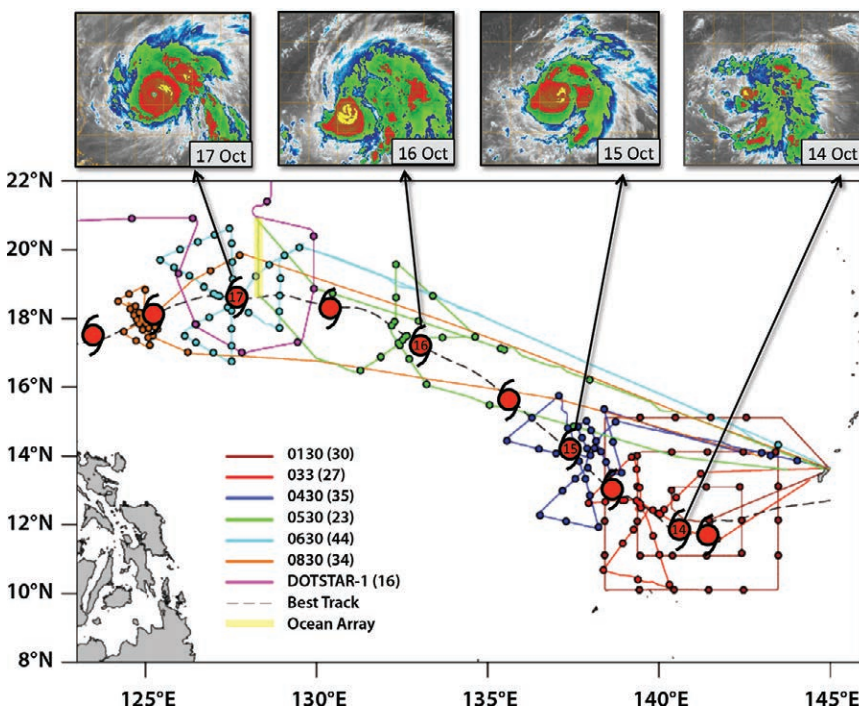
pre-Malakas disturbance initially also moved westward in the broad easterly flow. However, the storm turned sharply poleward under the influence of a deep midlatitude trough and then moved northward through varying ocean conditions, resulting in a more complex combination of atmospheric and oceanic factors affecting its intensity.

Figure 8 compares the convective structures and size of these three storms by superimposing typical airborne radar eye images: the eyewall of Megi fits inside the eyewall of Fanapi, which in turn fits inside the eyewall of Malakas. With respective eye diameters of 17, 44, and 130 km for Megi, Fanapi, and Malakas, the entire storm structure of Megi including the eyewall and rainbands fits within the eye of Malakas. This illustrates the large range of storm structures that are typical of TCs in the western Pacific and the corresponding differences in the size of the cold wakes produced.

The storm core structures also varied significantly (Table 1, Fig. 9). The core is characterized by the radius of maximum surface winds, the radius of flight-level (3 km) winds, the ratio of surface and flight-level maximum winds (Powell et al. 2009), and the slope defined by surface and flight-level wind maxima. These are computed from the difference in flight level (measured by WC-130J aircraft systems) and surface winds (measured by SFMR) near the time of maximum storm strength (Fig. 9, Table 1). For Typhoon Fanapi (Fig. 9a) the ratio of surface to flight level winds is 0.88 and the slope is 79 degrees. These values are similar to those of the typical hurricane over the North Atlantic (Powell et al. 2009; Hazelton and Hart 2013). Typhoon Malakas (Fig. 9b) has larger wind radii and a larger slope, but a smaller ratio of surface to flight-level winds. In contrast, Typhoon Megi (Fig. 9c) has smaller wind radii, a smaller slope, and a larger ratio of surface to flight-level winds.

OCEAN RESPONSES TO THE ITOP STORMS.
The cold wakes formed by the ITOP storms span a wide range of strengths and sizes (Fig. 10). Six wake events (Table 2)—the Fanapi, Malakas, and Megi wakes, a very different wake from Megi after it moved into the South China Sea (Megi-SC), a wake from Typhoon Lupit sampled by one of the moorings in 2009, and last the well-documented wake of Hurricane Frances (Sanford et al. 2011; D'Asaro
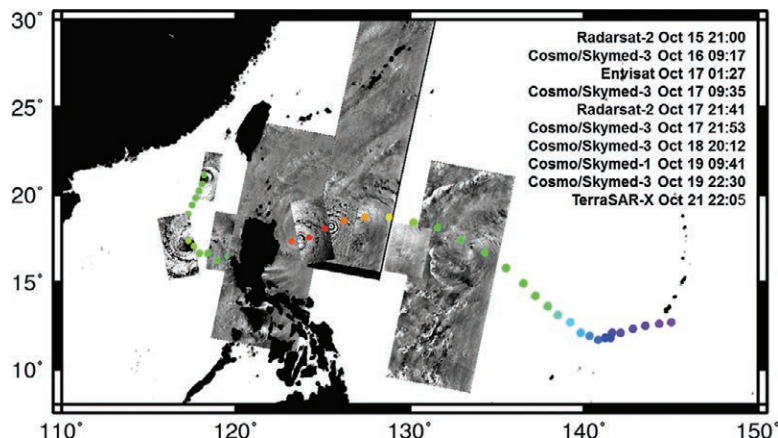

FIG. 7. Sequence of multisatellite radar data collections along the track of Typhoon Megi (dots).
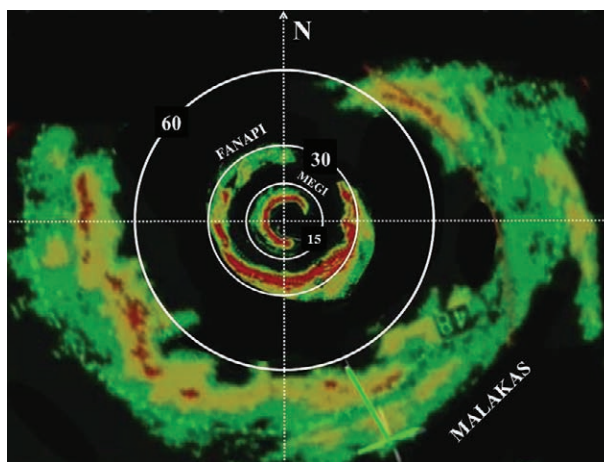

FIG. 8. Montage of airborne radar images of the eyewalls of typhoons Megi, Fanapi, and Malakas. Range rings are indicated by white circles with labels in km. The arrow indicates north.

et al. 2007)—are included in this analysis. Each storm's parameters are given for the time and location listed in Table 2 and marked by a star in each panel of Fig. 10.

Peak winds (U_{max}), from ITOP aircraft measurements if available or Cooperative Institute for Meteorological Satellite Studies (CIMSS) *SATCOM* estimates if not, span 41–70 m s^{-1}; the maximum stress likely spans a factor of about 2.5. The radius of maximum winds (R_{max}), from aircraft measurements if available or from CIMSS morphed imagery if not, span a factor of 4.5 (12–55 km) owing to the very small radius of Megi. Similarly, the storm translation speed (S) spans a factor of 3 (2.7–8 m s^{-1}), with Megi nearly stalling in the South China Sea and Malakas moving rapidly northward before undergoing extratropical transition. Ocean stratification, defined as the average temperature in the upper 100 m (T100), is estimated

from temperature profiles measured by ITOP floats, drifters, moorings, or Argo floats. The wake strength (i.e., cooling), defined as the difference between pre-storm SST to minimum wake temperature and estimated from a combination of ITOP measurements and microwave SST (Fig. 10), spans a factor of 4 (1.6°–7°C), with both extremes contributed by Megi. The wake width L_{wake} is estimated from the microwave images

and defined as the width with 66% of the cooling; it varies by a factor of 10 (23–222 km). The offset of the wake from the track R_{wake} (see cartoon in Fig. 13f) ranges from zero for Megi-SC, because this wake is nearly centered on the track, to 78 km for Malakas.

These data can test simple models of TC wakes. We assume that air–sea fluxes are unimportant compared to vertical mixing of the underlying oceanic stratification (Price 2009), although the ITOP data are certainly rich enough to relax this assumption in a more detailed analysis. Storm strength is not correlated with colder wakes; the strongest storm, Megi in the Philippine Sea (Megi-PS), has the weakest wake (Fig. 13a). Price (2009) assumes, as a first rough approximation, that all storms mix to 100 m; the resulting wake temperature $T100_0$ depends only on the ocean temperature profile, and the wake cooling is $\Delta T100 = SST_0 - T100_0$. This is indeed only approximately true; the Megi-SC wake is colder than predicted and thus must be mixed to much deeper than 100 m, while the Malakas wake must be mixed significantly less deep (Fig. 13b). Price (1981) implicitly assumes that the width of the cold wake (L_{wake}) is set by the storm size; the ITOP data show this trend, with the smallest storm, Megi-PS, having the narrowest wake (Fig. 13e).

A key dynamical parameter is the nondimensional storm speed $S/2 f R_{max}$, where f is the Coriolis frequency (Price 1981). For $S/2 f R_{max} < 1$, a "slow" storm, storm winds persist at a single location for longer than $1/f$, so that an Ekman balance can be established; the cyclonic stress from the storm diverges the warm surface water away from the track, replacing it by cold upwelled water and creating a cold wake centered on the track. In the limit of $S/2 f R_{max} = 0$, a stalled storm, upwelling continues indefinitely and the amount of cooling can be very large. In contrast, "fast" storms create a wake to the right of the storm track. Here the wind rotates clockwise with time and resonantly drives inertial currents in the mixed layer. The shear of these currents creates shear instability at the mixed layer base, leading to rapid mixed layer deepening. This is most effective for $S/2 f R_{max} \sim 1$, when the maximum winds are approximately resonant. The radius of resonance moves farther rightward with
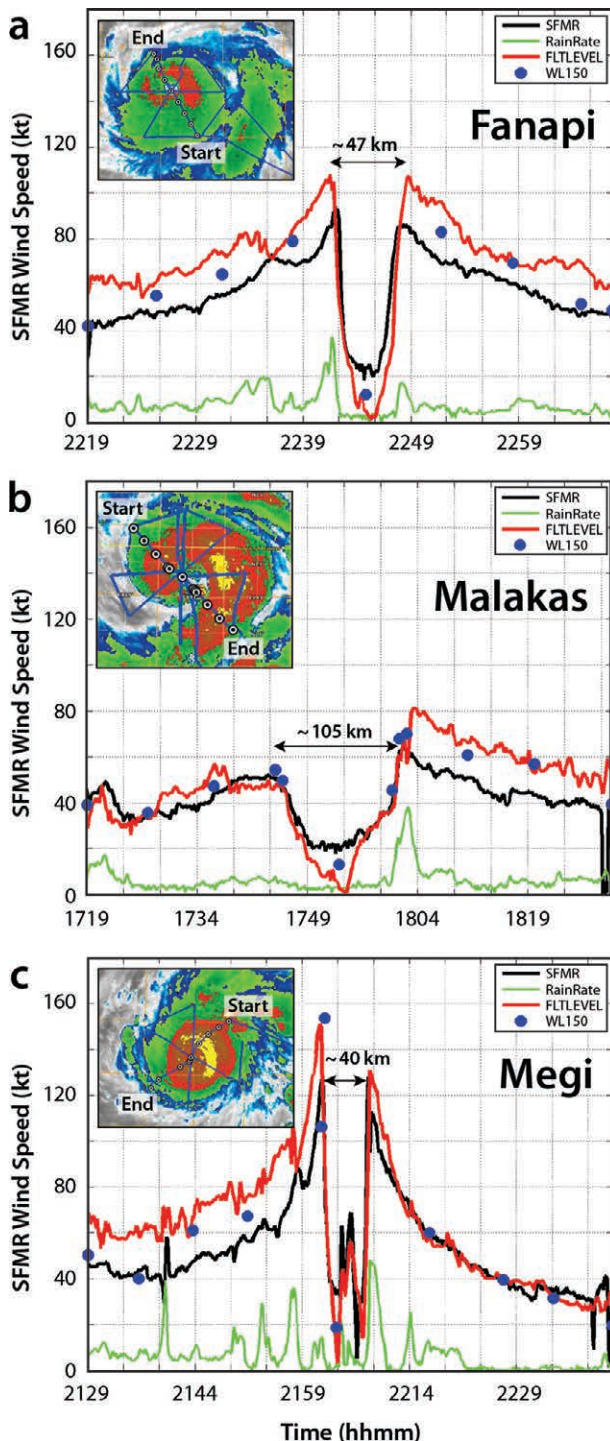

Fig. 9. Flight-level winds (kt, red line), surface winds (kt, black line), and surface rain rate (mm h⁻¹, green) for radial passes through (a) Typhoon Fanapi (flight 0620, pass 1), (b) Typhoon Malakas (0322 pass 2), and (c) Typhoon Megi (0630, pass 1). Solid blue dots are lowest 150-m dropsonde winds. The storm-relative flight track and dropsonde locations are shown on an MTSAT infrared image at the central time of the mission.

TABLE 2. Tropical cyclone wake properties.

	Date (2010), time, location	U_{max} (m s^{-1})	R_{max} (km)	Speed (m s^{-1})	Cooling (°C)	$\Delta T100$ (°C)	R_{wake} (km)	L_{wake} (km)
Typhoon Lupit	20 Oct 2009, 1200–1800 UTC, 20.4°N, 127.5°E	44*	54	4.4	3.8	1.8	39	167
Typhoon Fanapi	18 Sep, 0000 UTC, 23.5°N, 126.3°E	50**	21	4.5	2.5	1.6	49	150
Typhoon Malakas	24 Sep, 0000 UTC, 24°N, 142°E	41**	55	8	3	5	78	222
Supertyphoon Megi-PS	16 Oct, 2000 UTC, 19°N, 128.4° E	70**	12	7	1.6	2	56	23
Supertyphoon Megi-SC	20 Oct, 1600 UTC, 19°N, 117°E	56*	55	2.7	7	2.7	0	222
Hurricane Frances	1 Sep 2004, 1800 UTC, 22°N 70°W	65*	40	6	2.1	1.4	75	111

* From CIMSS.

** From aircraft.

increasing storm speed, increasing the asymmetry of the wake, but also decreasing the magnitude of the currents, the mixing caused by them, and thus the amount of cooling. Figure 13d confirms the increasing rightward bias with increasing values of $S/2 f R_{max}$. This can also be seen in Fig. 10: Megi-SC, the slowest storm, has a symmetrical wake whereas Megi-PS, Fanapi, and Malakas, all faster storms, have asymmetrical wakes. A remarkably strong dependence of wake cooling on $S/2 f R_{max}$ (Fig. 13c) confirms the importance of this parameter. However, because the amount of cooling must also be influenced by the ocean stratification, the nearly perfect correlation in Fig. 13c must be at least partially due to the particular storms chosen and is not a general result.

Many features of the wakes are not captured by this simple analysis. The increasingly cold wake of Malakas to the north, despite its increasing speed, is probably due to the increasingly colder upper ocean temperatures. The lack of a cold wake in Megi-PS at its peak before encountering the Philippines, the cold circular feature in Fanapi's wake near its
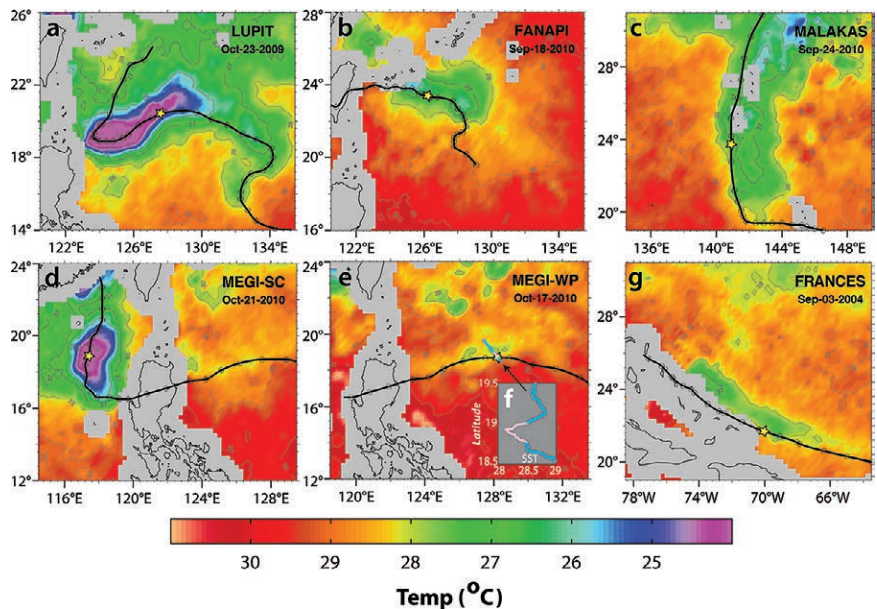

FIG. 10. (a)–(f) SST wakes of the ITOP storms. Color shows optimally mapped microwave SST (www.remss.com). Black line is the International Best Track Archive for Climate Stewardship (IBTrACS) storm track (Knapp et al. 2010) up to one day after the time of the map. Star shows region of wake analyzed here. Insert (f) shows SST across the very narrow wake of Megi as measured by the R/V _Revelle_ on 17–20 Oct. (g) The wake of Atlantic Hurricane Frances. All panels use the same color map for temperature and are plotted on the same spatial scale.

southern edge, and the very strong wake of Lupit near its northward turn (Fig. 10a) could easily be due to additional variability in the ocean and complexities in the storm track.

EVOLUTION OF STORM COLD WAKES.
ITOP measured the evolution of Typhoon Fanapi's cold wake for more than 3 weeks after the storm passage (Mrvaljevic et al. 2014). Figure 11 shows

the evolution of upper ocean stratification at approximately the center of the wake. Mixing to about 100 m is apparent on day 261 (18 September 2010) as the storm passes over, creating an approximately 110-m-thick, 26°C mixed layer. This layer was capped by a warm layer within 3 days and thus becomes increasingly invisible in satellite SST measurements, most likely owing to the increased air–sea heat flux into the colder wake SST (Price et al. 2008). The cap created a subsurface layer that ITOP tracked for 37

days until it was mixed into the surface layer by the passage of Typhoon Chaba on 28 October. During this time, the surface layer thinned with an *e*-folding time of 23 days and was carried up to 300 km away from its generation site by the energetic eddies in this region.

The evolution of the Malakas cold wake has a similar pattern (Fig. 12). Mixing during the storm created an approximately 45-m-thick, 28°C mixed layer at the center of the wake (Fig. 12c). This layer was capped by a warm layer; the subsurface cold layer then thinned. After about 13 days the wake disappeared from Autonomous Drifting Ocean Stations (ADOS) observations (Fig. 12). During this time, the wake was distorted by the mesoscale eddy field. The southern edge of the wake moved northward; its western edge moved eastward, especially near 26°N (Figs. 12a,b). These displacements correspond to the oceanic velocity field (arrows) and the displacement of the drifter (white line). Similarly, a float deployed in Megi's western wake (e.g., Fig. 10e) observed a brief episode of capping within 12 h with a permanent cap forming 36 h after the storm passage (not shown here). A ship section across Megi's wake in
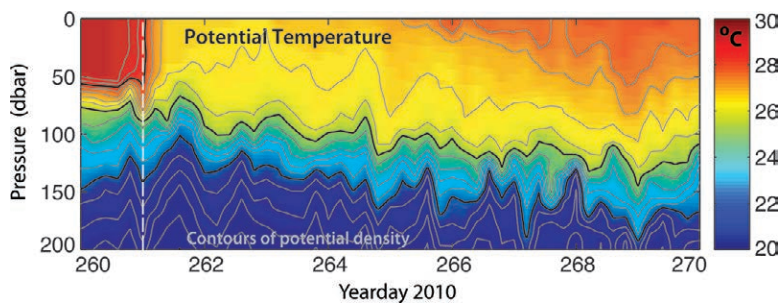

FIG. 11. Evolution of the Typhoon Fanapi wake. Potential temperature measured by a profiling EM-APEX float deployed near the center of the cold wake of Typhoon Fanapi. The storm creates a cold wake that is then capped by a thin, warm surface layer, but persists beneath this layer.
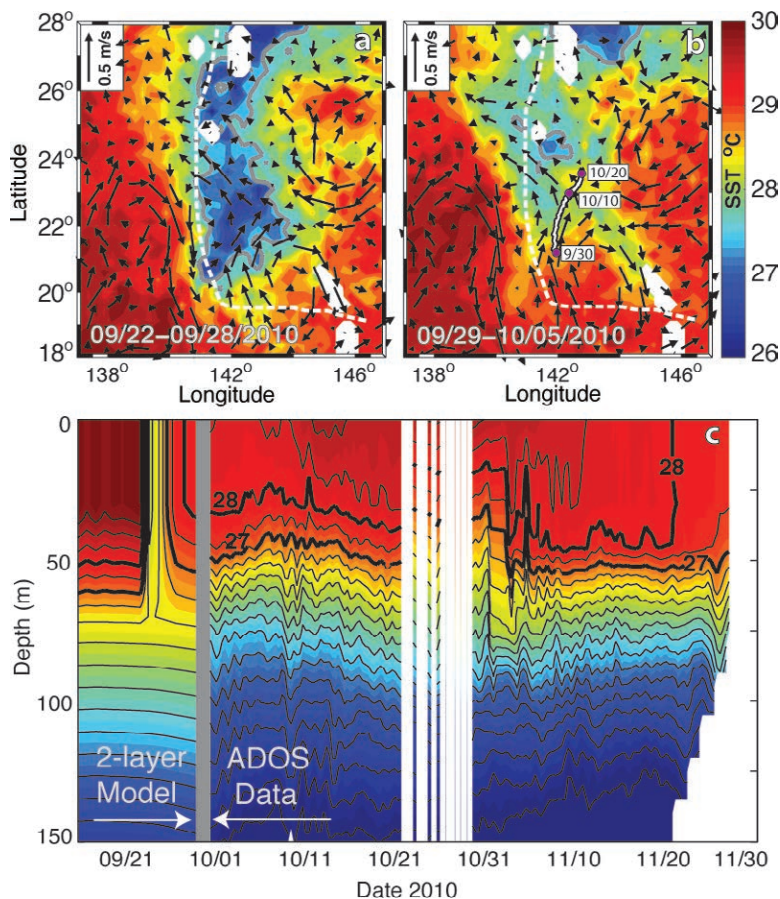

FIG. 12. Evolution of the Typhoon Malakas wake. (a),(b) Mean SST from the Tropical Rainfall Measuring Mission (TRMM) Microwave Imager (TMI) (www.remss.com), with contoured 27.5°C isotherm (gray) and overlaid geostrophic velocity anomalies from Archiving, Validation, and Interpretation of Satellite Oceanographic data (AVISO; Le Traon et al. 1998, black vectors) for the weeks of (a) 22 and (b) 29 Sep 2010, respectively. Track of ADOS drifter 82326 is superimposed (white); circles show position on 30 Sep and 10 and 20 Oct. White dashed line shows track of Typhoon Malakas. (c) Depth–time in situ temperature from drifter 82326 starting on about 30 Sep (colors and contours). Data before 30 Sep are computed using the two-layer model following Pun et al. (2007) based on satellite data and the Monthly Isopycnal and Mixed-Layer Ocean Climatology (Schmidtko et al. 2013) applied at the drifter deployment location.

the South China Sea (e.g., Fig. 10d) observed a capped wake 5 days after the storm passage. A mooring beneath Typhoon Lupit (e.g., Fig. 10a) observed a capped wake persisting for 10 days. In almost all cases, the actual wake lifetime may have been longer than observed because the wake could have moved away from the measurement platforms or persisted longer than the observations.

The ITOP data thus show that subsurface typhoon wakes, characterized by a subsurface minimum in stratification with the temperature of the storm's initial cold wake, are common. These features are 20–100 m thick with typical lifetimes of 10–30 days and they can be advected hundreds of kilometers from the storm track. Their decay is substantially faster than that expected from estimates of the ambient vertical diffusivity (10^{-4} m^2 s^{-1} over 20 days diffuses 13 m), suggesting that other mechanisms may be important in controlling their lifetime. For these late season storms, an ultimate lifetime of one month or so is set by the seasonal deepening of the mixed layer past the depth of the wake.

FIG. 13. Relationships between different properties of the six wakes in Fig. 10 and Table 2. (a) Wake cooling vs maximum wind. (b) Wake cooling vs $\Delta T100$. (c) Wake cooling vs nondimensional storm speed. (d) Ratio of wake offset to R_{max} vs nondimensional storm speed. (e) Ratio of wake width to 2 R_{max}. (f) Graphical key to wake and storm properties. Dashed lines show 1:1 relationship in (b) and (e), and $4/(S/2\,f\,R_{max})^{1/2}$ in (c).

OCEAN CONTROLS ON AIR–SEA FLUXES.

ITOP was able to estimate directly the oceanic influence on air–sea fluxes by measuring ocean and atmospheric properties simultaneously using pairs of dropsondes and AXBTs deployed in each storm's inner core. Despite very similar warm (~29.5°C) precyclone SST (Figs. 2, 14a), the three ITOP typhoons developed in very different ocean environments, as shown by the profiles (Fig. 14a) and the corresponding differences in T100 (Fig. 1). Their contrasting development illustrates how differences in subsurface ocean thermal structure modify air–sea fluxes with potential impacts on typhoon intensity (Lin et al. 2013).

Typhoon Megi intensified over an unusually deep, thick subsurface warm layer (Fig. 14a) deepened
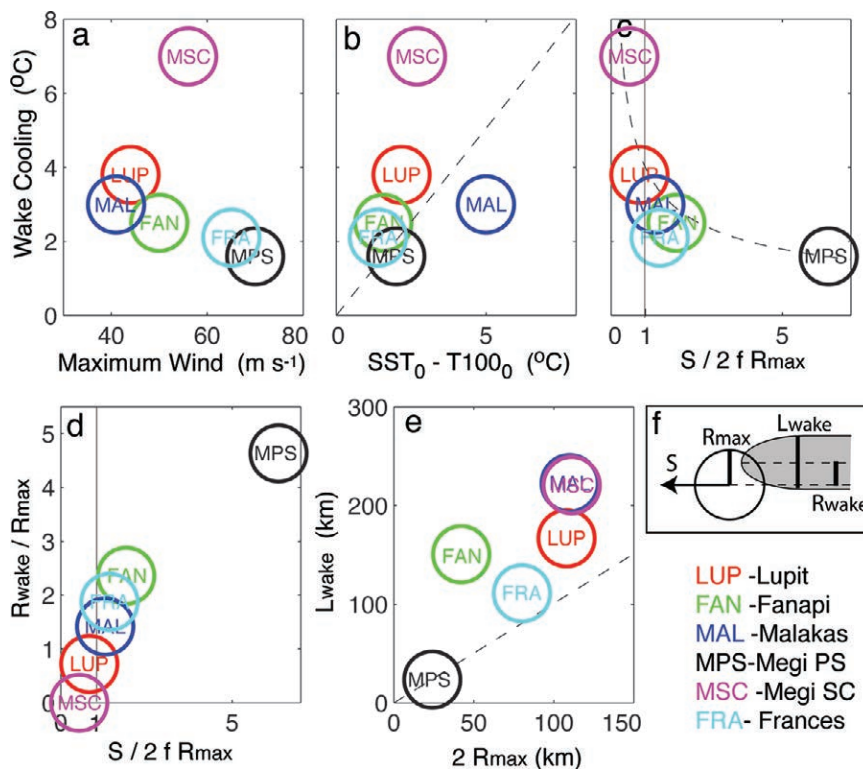
from the already-deep baseline climatological values due to the 2010 La Niña. Because of this thick warm layer, Megi's fast translation speed, and its small size (Fig. 13d), SST beneath Megi cooled little (Fig. 14b). With SST remaining near 29°C and inner core air temperatures of ~27°C, air–sea temperature differences of ~2°C and corresponding humidity differences were maintained throughout Megi's intensification period. Enthalpy fluxes (Fig. 14c) increased with wind speed, thereby allowing the storm to intensify to its maximum potential (Emanuel 1988; Lin et al. 2013).

Typhoons Fanapi and Malakas intensified over regions with much shallower warm layers (Fig. 14a) and correspondingly lower T100 values (Fig. 1). This and their slower propagation speeds (Fig. 13c) resulted in SST cooling by 1°–2°C during intensification (Fig. 14b). For Fanapi, core air temperatures remained near 27°C, so the air–sea temperature differences decreased dramatically, reaching nearly zero at its peak wind of ~55 m s⁻¹. Humidity differences also decreased so that the total air–sea enthalpy flux (Fig. 14c) is less than half of Megi's flux at the same wind speed. The situation is similar, if less dramatic, for Malakas.
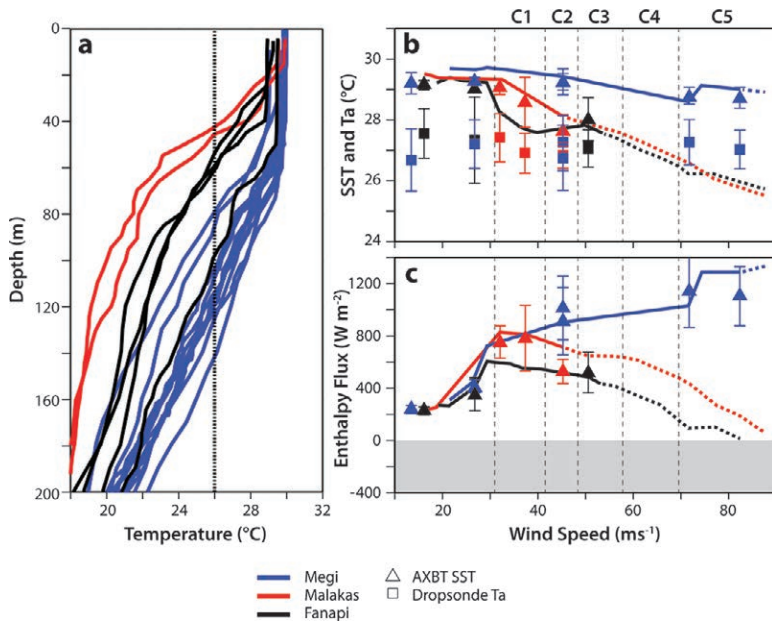
FIG. 14. Evolution of temperature and air–sea fluxes for three ITOP storms. (a) Prestorm temperature profiles for each ITOP storm from ARGO floats. (b) Symbols: SST and air temperature at the core of each storm as measured by dropsonde/AXBT pairs. Lines: results of an ocean model driven by the observed storms (solid) and extrapolated to higher wind speeds (dashed). (c) As in (b), but for estimated total enthalpy flux. Some of the AXBT profiles may be ~5 m shallow. Figure adapted from Lin et al. (2013).

Additional insight is obtained by simulating the additional reduction in core SST resulting from further storm intensification [Figs. 14b,c, dashed lines; see Lin et al. (2013) for details]. For Fanapi, SST decreases below the core air temperature, reversing the sign of the sensible heat flux and bringing the total flux to zero at a hypothetical wind speed of ~80 m s^{-1}. This reduction in core fluxes due to ocean cooling may play an important role in limiting the intensities of Fanapi and Malakas relative to Megi (Lin et al. 2013).

More detailed studies show other mechanisms by which ocean cooling influences TC structure. Dropsonde data collected in Typhoon Fanapi show the development of a stable boundary layer in the atmosphere over the colder SST in the right rear quadrant. This layer suppresses the transport of near-surface air into rainbands downstream of the cold SST, keeping air parcels near the warm ocean surface longer and increasing the inward turning of the wind over and downstream of the cold wake, a feature supported by results from high-resolution coupled atmosphere–ocean models (Chen et al. 2013; Lee and Chen 2014).

PERSPECTIVE. ITOP contained many more elements than can be addressed here. In particular,

the experimental team worked closely with a modeling team, which included atmospheric, oceanic, and coupled variants. We have not addressed more detailed observations of ocean velocity or air–sea fluxes.

ITOP involved close cooperation between oceanographers and meteorologists and thus resulted in oceanic and atmospheric data fields measured on the same spatial scales. This allowed an analysis of the links between ocean dynamics, driven by storm fluxes, to SST and flux changes, and the resulting influences on the storm intensity. This cooperation was made possible by the rapid advances in technology available to measure the atmosphere and ocean under tropical cyclone conditions. Aircraft deployments of oceanographic and atmospheric probes and the ability to position long-lived ocean floats and drifters precisely into storms allows researchers to address the issues of air–sea interaction in these storms in fresh detail and examine the longer-term fate of the ocean perturbations introduced by the storms. Placement of these sensors greatly benefited from high-resolution models of both the ocean and atmosphere. Continued advances in understanding the interaction between the ocean and tropical cyclones will rely on continuing progress in the ability to make such observations, the ability to model these phenomena, and the clever use of these abilities by coordinated scientific teams.

authors also thank the entire ITOP team, including the U.S. Air Force Reserve Command 53rd Weather Reconnaissance Squadron "Hurricane Hunters," the captains and crews of the U.S. and Taiwanese research vessels, our forecast team, and the many engineers, technicians, programmers, and support personnel that made the work possible.

REFERENCES

Black, P. G., 1983: Ocean temperature changes induced by tropical cyclones. Ph.D. thesis, The Pennsylvania State University, 278 pp.

——, and Coauthors, 2007: Air–sea exchange in hurricanes: Synthesis of observations from the Coupled Boundary Layer Air–Sea Transfer experiment. *Bull. Amer. Meteor. Soc.,* **88,** 357–374, doi:10.1175/BAMS -88-3-357.

Centurioni, L. R., 2010: Observations of large-amplitude nonlinear internal waves from a drifting array: Instruments and methods. *J. Atmos. Oceanic Technol.,* **27,** 1711–1731, doi:10.1175/2010JTECHO774.1.

Chen, S. S., J. F. Price, W. Zhao, M. A. Donelan, and E. J. Walsh, 2007: The CBLAST-hurricane program and the next-generation fully coupled atmosphere–wave– ocean models for hurricane research and prediction. *Bull. Amer. Meteor. Soc.,* **88,** 311–317, doi:10.1175 /BAMS-88-3-311.

——, W. Zhao, M. A. Donelan, and H. L. Tolman, 2013: Directional wind–wave coupling in fully coupled atmosphere–wave ocean models: Results from CBLAST-hurricane. *J. Atmos. Sci.,* **70,** 3198–3215, doi:10.1175/JAS-D-12-0157.1.

D'Asaro, E. A., and C. McNeil, 2007: Air–sea gas exchange at extreme wind speeds measured by autonomous oceanographic floats. *J. Mar. Syst.,* **66,** 92–109, doi:10.1016/j.jmarsys.2006.06.007.

——, T. B. Sanford, P. P. Niiler, and E. J. Terrill, 2007: Cold wake of Hurricane Frances. *Geophys. Res. Lett.,* **34,** L15609, doi:10.1029/2007GL030160.

Emanuel, K. A., 1988: The maximum intensity of hurricanes. *J. Atmos. Sci.,* **45,** 1143–1155, doi:10.1175/1520 -0469(1988)0452.0.CO;2.

——, 1999: Thermodynamic control of hurricane intensity. *Nature,* **401,** 665–669, doi:10.1038/44326.

Eriksen, C. C., T. J. Osse, R. D. Light, T. Wen, T. W. Lehman, P. L. Sabin, and A. M. Chiodi, 2001: Seaglider: A long-range autonomous underwater vehicle for oceanographic research. *IEEE J. Oceanic Eng.,* **26,** 424–436, doi:10.1109/48.972073.

Foster, R. C., 2013: Signature of large aspect ratio roll vortices in synthetic aperture radar images of tropical cyclones. *Oceanography,* **26,** 58–67, doi:10.5670 /oceanog.2013.31.

Graber, H. C., E. A. Terray, M. A. Donelan, W. M. Drennan, J. C. Van Leer, and D. B. Peters, 2000: ASIS—A new air–sea interaction spar buoy: Design and performance at sea. *J. Atmos. Oceanic Technol.,* **17,** 708–720, doi:10.1175/1520-0426 (2000)0172.0.CO;2.

Hazelton, A. T., and R. E. Hart, 2013: Hurricane eyewall slope as determined from airborne radar reflectivity data: Composites and case studies. *Wea. Forecasting,* **28,** 368–386, doi:10.1175/WAF -D-12-00037.1.

Hong, X., S. W. Chang, S. Raman, L. K. Shay, and R. Hodur, 2000: The interaction between Hurricane Opal (1995) and a warm core ring in the Gulf of Mexico. *Mon. Wea. Rev.,* **128,** 1347–1365, doi:10.1175/1520-0493(2000)1282.0.CO;2.

Horstmann, J., W. Koch, S. Lehner, and R. Tonboe, 2000: Wind retrieval over the ocean using synthetic aperture radar with C-band HH polarization. *IEEE Trans. Geosci. Remote Sens.,* **38,** 2122–2131, doi:10.1109/36.868871.

——, D. R. Thompson, F. Monaldo, S. Iris, and H. C. Graber, 2005: Can synthetic aperture radars be used to estimate hurricane force winds? *Geophys. Res. Lett.,* **32,** L22801, doi:10.1029/2005GL023992.

——, C. Wackerman, S. Falchetti, and S. Maresca, 2013: Tropical cyclone winds retrieved from synthetic aperture radars. *Oceanography,* **26,** 46–57, doi:10.5670/oceanog.2013.30.

Jaimes, B., and L. K. Shay, 2009: Mixed layer cooling in mesoscale oceanic eddies during Hurricanes Katrina and Rita. *Mon. Wea. Rev.,* **137,** 4188–4207, doi:10.1175/2009MWR2849.1.

——, and ——, 2010: Near-inertial wave wake of Hurricanes Katrina and Rita over mesoscale oceanic eddies. *J. Phys. Oceanogr.,* **40,** 1320–1337, doi:10.1175/2010JPO4309.1.

Knapp, K. R., M. C. Kruk, D. H. Levinson, H. J. Diamond, and C. J. Neumann, 2010: The International Best Track Archive for Climate Stewardship (IBTrACS): Unifying tropical cyclone data. *Bull. Amer. Meteor. Soc.,* **91,** 363–376, doi:10.1175/2009BAMS2755.1.

Lee, C.-Y, and S. S. Chen, 2014: Stable boundary layer and its impact on tropical cyclone structure in a coupled atmosphere–ocean model. *Mon. Wea. Rev.,* **142,** 1927–1944, doi:10.1175/MWR-D-13-00122.1.

Leipper, D. F., 1967: Observed ocean conditions and Hurricane Hilda, 1964. *J. Atmos. Sci.,* **24,** 182–186, doi:10.1175/1520-0469(1967)0242.0.CO;2.

Le Traon, P. Y., F. Nadal, and N. Ducet, 1998: An improved mapping method of multisatellite altimeter data. *J. Atmos. Oceanic Technol.,* **15,** 522–534, doi:10.1175/1520-0426(1998)0152.0.CO;2.

Lévy, M., M. Lengaigne, L. Bopp, E. M. Vincent, G. Madec, C. Ethé, D. Kumar, and V. V. S. S. Sarma, 2012: Contribution of hurricanes to the air–sea CO_2 flux: A global view. *Global Biogeochem. Cycles,* **26**, GB2001, doi:10.1029/2011GB004145.

Lin, I.-I., C.-C. Wu, K. A. Emanuel, I. H. Lee, C.-R. Wu, and I.-F. Pun, 2005: The interaction of Supertyphoon Maemi (2003) with a warm ocean eddy. *Mon. Wea. Rev.,* **133**, 2635–2649, doi:10.1175 /MWR3005.1.

——, ——, I. F. Pun, and D. S. Ko, 2008: Upper-ocean thermal structure and the western North Pacific category 5 typhoons. Part I: Ocean features and the category 5 typhoons' intensification. *Mon. Wea. Rev.,* **136**, 3288–3306, doi:10.1175/2008MWR2277.1.

——, and Coauthors, 2013: An ocean coupling potential intensity index for tropical cyclones. *Geophys. Res. Lett.,* **40**, 1878–1882, doi:10.1002/grl.50091.

Mrvaljevic, R. K., and Coauthors, 2014: Observations of the cold wake of Typhoon Fanapi (2010). *Geophys. Res. Lett.,* doi:10.1002/grl.50096, in press.

Niiler, P. P., 2001: The world ocean surface circulation. *Ocean Circulation and Climate,* G. Siedler et al., Eds., Academic Press, 193–204.

Patoux, J., R. C. Foster, and R. A. Brown, 2008: An evaluation of scatterometer-derived oceanic surface pressure fields. *J. Appl. Meteor. Climatol.,* **47**, 835–852, doi:10.1175/2007JAMC1683.1.

Powell, M. D., E. W. Uhlhorn, and J. D. Kepert, 2009: Estimating maximum surface winds from hurricane reconnaissance measurements. *Wea. Forecasting,* **24**, 868–883, doi:10.1175/2008WAF2007087.1.

Price, J. F., 1981: Upper ocean response to a hurricane. *J. Phys. Oceanogr.,* **11**, 153–175, doi:10.1175/1520 -0485(1981)0112.0.CO;2.

——, 2009: Metrics of hurricane–ocean interaction: Vertically-integrated or vertically-averaged ocean temperature? *Ocean Sci.,* **5**, 351–368, doi:10.5194 /os-5-351-2009.

——, J. Morzel, and P. P. Niller, 2008: Warming of SST in the cold wake of a moving hurricane. *J. Geophys. Res.,* **113**, C07010, doi:10.1029/2007JC004393.

Pudov, V., and S. Petrichenko, 2000: Trail of a typhoon in the salinity field of the ocean upper layer. *Atmos. Ocean Phys.,* **36**, 700–706.

Pun, I.-F., I.-I. Lin, C.-R. Wu, D.-S. Ko, and W. T. Liu, 2007: Validation and application of altimetry-derived upper ocean thermal structure in the western North Pacific Ocean for typhoon-intensity forecast. *IEEE Trans. Geosci. Remote Sens.,* **45**, 1616–1630, doi:10.1109/TGRS.2007.895950.

——, Y.-T. Chang, I.-I. Lin, T. Y. Tang, and R.-C. Lien, 2011: Typhoon–ocean interaction in the western North Pacific, Part 2. *Oceanography,* **24**, 32–41, doi:10.5670/oceanog.2011.92.

Romeiser, R., J. Horstmann, M. J. Caruso, and H. C. Graber, 2013: A descalloping post-processor for ScanSAR images of ocean scenes. *IEEE Trans. Geosci. Remote Sens.,* **51**, 3259–3272, doi:10.1109 /TGRS.2012.2222648.

Sanford, T. B., J. F. Price, and J. B. Girton, 2011: Upper-ocean response to Hurricane Frances (2004) observed by profiling EM-APEX floats. *J. Phys. Oceanogr.,* **41**, 1041–1056, doi:10.1175/2010JPO4313.1.

Schmidtko, S., G. C. Johnson, and J. M. Lyman, 2013: MIMOC: A global monthly isopycnal upper-ocean climatology with mixed layers. *J. Geophys. Res.,* **118**, 1658–1672, doi:10.1002/jgrc.20122.

Schulz-Stellenfleth, J., and S. Lehner, 2004: Measurement of 2D sea surface elevation fields using complex synthetic aperture radar data. *IEEE Trans. Geosci. Remote Sens.,* **42**, 1149–1160, doi:10.1109 /TGRS.20O4.826811.

Shay, L. K., 2010: Air–sea interactions in tropical cyclones. *Global Perspectives on Tropical Cyclones: From Science to Mitigation,* J. C. L. Chan and J. D. Kepert, Eds., World Scientific, 93–131.

Uhlhorn, E. W., P. G. Black, J. L. Franklin, M. Goodberlet, J. Carswell, and A. S. Goldstein, 2007: Hurricane surface wind measurements from an operational stepped frequency microwave radiometer. *Mon. Wea. Rev.,* **135**, 3070–3085, doi:10.1175 /MWR3454.1.

Wackerman, C. C., C. L. Rufenach, R. A. Shuchman, J. A. Johannessen, and K. L. Davidson, 1996: Wind vector retrieval using ERS-1 synthetic aperture radar imagery. *IEEE Trans. Geosci. Remote Sens.,* **34**, 1343–1352, doi:10.1109/36.544558.

Wright, C. W., and Coauthors, 2001: Hurricane directional wave spectrum spatial variation in the open ocean. *J. Phys. Oceanogr.,* **31**, 2472–2488, doi:10.1175/1520-0485(2001)0312.0.CO;2.

Wu, C.-C., and Coauthors, 2005: Dropwindsonde Observations for Typhoon Surveillance near the Taiwan Region (DOTSTAR): An overview. *Bull. Amer. Meteor. Soc.,* **86**, 787–790, doi:10.1175/BAMS -86-6-787.

Yablonsky, R. M., and I. Ginis, 2013: Impact of a warm ocean eddy's circulation on hurricane-induced sea surface cooling with implications for hurricane intensity. *Mon. Wea. Rev.,* **141**, 997–1021, doi:10.1175 /MWR-D-12-00248.1.